

Transition Pathways of One-Dimensional Cholesteric Liquid Crystals

Yucen Han², James Dalby², Benjamin MGD Carter¹, Apala Majumdar² and Thomas Machon¹.

¹*H.H. Wills Physics Laboratory, University of Bristol,
Tyndall Avenue, Bristol BS8 1TL, United Kingdom and*

²*Department of Mathematics and Statistics, University of Strathclyde,
Livingstone Tower, 26 Richmond Street, Glasgow G1 1XH, United Kingdom*

Cholesteric liquid crystals exhibit great morphological richness of static metastable states, yet the transitions between these states, key for switchable devices, remains unstudied. We consider a simple cholesteric cell and study the energy landscape and transition pathways under quasi-one-dimensional assumption. For distinct minima distinguished by chiral topological invariants, we show that transition pathways can be driven by either splay-mediated untwisting or biaxiality. Our work suggests a simple route to experimental observation of biaxiality.

Cholesteric liquid crystals display rich morphology, particularly in confinement. For a given geometry, with specified boundary conditions, one typically finds a huge variety of metastable states. These include arbitrarily knotted disclination lines [1–4], torons [5, 6] and hopf solitons [7], inverse torons [8], point defect constellations [9, 10], complex patterns in shells and droplets [11–14], and Skyrmion lattices [15] amongst many others. This richness gives cholesteric liquid crystals great potential for the creation of soft devices. There is another key strength to cholesterics and all liquid crystal systems, they flow (spontaneously in the case of active systems) and readily respond to applied fields [16]; in other words, they are switchable. For a switchable device, understanding and controlling pathways between stable states is just as important as understanding the stable states themselves, non energy-minimizing critical points play crucial roles in switching mechanics and selection of minimizers [17]. In a cholesteric system, chirality leads to many complex metastable configurations and one expects similar richness in the space of transition pathways between metastable states, something which has not yet received much attention for liquid crystals although there has been recent interesting work for transition pathways between metastable nematic states on 2D polygons in [17].

Many liquid crystalline configurations are distinguished by their topology, using homotopy theoretic approaches [18–20]. Homotopy theoretic invariants however, often cannot distinguish between two cholesteric configurations that appear qualitatively distinct. The simplest example [21], and the one considered here, is the number of layers in a cholesteric cell, with all even (or odd) layer numbers equivalent from a homotopy theoretic perspective. An alternative approach uses ideas from contact topology [8, 10, 21] to provide more sophisticated chiral invariants that *can* distinguish such configurations. In this theory, the key role is played by the twist density $\mathbf{n} \cdot \nabla \times \mathbf{n}$, with \mathbf{n} the nematic director. If the twist density is nowhere-zero, we say the liquid crystal configuration is chiral. Using the tools of contact topology [22] one can rigorously define new invariants (e.g. the layer number [8, 21, 23]) which can distinguish chiral configurations (for example helices with different

numbers of twists). In particular, this theory implies that any pathway between configurations with different chiral invariants must either pass through an achiral untwisted configuration, where the twist vanishes at some given point, a biaxial configuration and/or proceed via defects, with both options energetically unfavorable.

As such, we can expect transition states between different ‘chiral sectors’ of the cholesteric landscape to contain topologically interesting untwisted configurations. In this work, we study a model cholesteric system, a simple twisted cell of height h , chosen to be tractable yet of sufficient complexity to capture much interesting behaviour.

We consider pathways between metastable cholesteric twisted states, with different chiral invariants, and study the competition between pathways which untwist (uniaxial pathways) and those which involve defects accompanied by biaxiality. In doing so, we capture both the diversity of metastable cholesteric states and the diversity of the unstable states that connect the metastable states, dictating the connectivity of the landscape. There are simple recurring structural motifs in the corresponding solution landscapes of this model system, and these motifs influence the symmetries, singularities and stability properties of cholesteric configurations. Additionally, we explore the interplay between geometry and material constants in the solution landscapes, and in doing so, identify conditions which could facilitate the experimental observation of biaxiality, a problem of contemporary interest for new material phases e.g. blue phases, fast-switching devices and composite materials [5].

We consider a cholesteric cell modelled by $\Omega = \{(x, y, z) \in \mathbb{R}^3 \mid 0 \leq z \leq h\} \subset \mathbb{R}^3$. The cholesteric state is described by the LdG \mathbf{Q} -tensor, expressed in Cartesian coordinates as a traceless symmetric 3×3 matrix \mathbf{Q} with components Q_{ij} . The eigenvector of \mathbf{Q} , with the largest positive eigenvalue, is the nematic director [24]. Assuming the \mathbf{Q} tensor is invariant under translations in the x and y directions, we obtain an effectively one-dimensional (1D) system. Rescaling using $z = \bar{z}h$ yields the non-

dimensionalized cholesteric energy per unit area [25]

$$\bar{F}(\mathbf{Q}) = \frac{hF(\mathbf{Q})}{K_0} = \int_0^1 \left\{ \frac{1}{4}(\bar{\nabla} \cdot \mathbf{Q})^2 + \frac{\eta}{4} |\bar{\nabla} \times \mathbf{Q} + 2\sigma \mathbf{Q}|^2 + \lambda \frac{f_b(\mathbf{Q})}{C} \right\} d\bar{z}. \quad (1)$$

The elastic energy density has splay and twist contributions: $\eta = K_1/K_0$ is the ratio of the twist and splay elastic constants and quantifies the elastic anisotropy; $\sigma/2\pi = h/p_0$ where p_0 is the pitch of the cholesteric, gives the number of 2π rotations of the director in the z -direction; and $\lambda = \frac{h^2 C}{K_0}$ is a measure of domain height/size with C a material-dependent positive constant. Henceforth, we omit bars from rescaled variables. The bulk energy density is

$$f_b(\mathbf{Q}) := \frac{A}{2} \text{tr} \mathbf{Q}^2 - \frac{B}{3} \text{tr} \mathbf{Q}^3 + \frac{C}{4} (\text{tr} \mathbf{Q}^2)^2, \quad (2)$$

and dictates the isotropic-nematic phase transition as a function of temperature. The variable $A = \alpha(T - T^*)$ is a rescaled temperature, with T^* a characteristic temperature, and $B, C > 0$ are material dependent constants [24]. We work with low temperatures for which $A < 0$, so the set of bulk energy minimizers are uniaxial \mathbf{Q} -tensors of the form $\mathbf{Q} = s_+(\mathbf{n} \otimes \mathbf{n} - \mathbf{I}/3)$. Here \mathbf{I} is the 3×3 identity matrix, $s_+ = (B + \sqrt{B + 24|A|C})/4C$, and $\mathbf{n} \in \mathbb{S}^2$ is arbitrary [26]. We impose Dirichlet boundary conditions on the top and bottom of the cell ($z = 0$ and $z = h$) given by $\mathbf{Q}(z = 0) = \mathbf{Q}(z = h) = s_+(\mathbf{e}_x \otimes \mathbf{e}_x - \mathbf{I}/3)$, where \mathbf{e}_x is a unit vector in the x -direction. This is equivalent to including a Rapini-Papoular surface energy in the limit of infinite surface anchoring. The physically observable configurations correspond to either local or global minimizers of (1), subject to the Dirichlet conditions.

For uniaxial systems, the LdG \mathbf{Q} -tensor has a pair of degenerate eigenvalues with three remaining degrees of freedom, and the minimizers are single-twist helical states [27]. We can study these analytically by taking the $\lambda \rightarrow \infty$ limit (i.e., $h \rightarrow \infty$), corresponding to a very tall cell. The bulk term becomes dominant and, informally speaking, the energy minimizers are solutions of the Euler-Lagrange equations in the restricted space of bulk energy minimizers, \mathcal{N} [28]. One can check that the leading order minimizer profiles are

$$\mathbf{Q}_\omega(z) := s_+ \left(\mathbf{n} \otimes \mathbf{n} - \frac{1}{3} \mathbf{I} \right), \quad \mathbf{n} = (\cos(\omega\pi z), \sin(\omega\pi z), 0), \quad (3)$$

for any $\omega \in \mathbb{Z}$. Substituting \mathbf{Q}_ω into (1), yields a quadratic in ω , minimized when $\omega = \frac{\sigma}{\pi}$. The limit of large elastic anisotropy is captured by $\eta \rightarrow \infty$ and one can check that the limiting profile of the energy minimizers (away from the boundary) is the biaxial helix [27]

$$\mathbf{Q}_b(z) = \frac{\lambda_1}{2} \begin{pmatrix} \cos(2\sigma z) & \sin(2\sigma z) & 0 \\ \sin(2\sigma z) & -\cos(2\sigma z) & 0 \\ 0 & 0 & 0 \end{pmatrix}. \quad (4)$$

If we allow dependence on all Cartesian coordinates, then linear combinations of the biaxial helices of varying orientations give the blue phases [27].

Notably, solutions in the $\lambda \rightarrow \infty$ and $\eta \rightarrow \infty$ limits have zero splay or $Q_{13} = Q_{23} = 0$. Splay deformations typically carry a higher energetic cost than twist, and so it is of interest to consider the zero splay limit, $K_0 \rightarrow \infty$, equivalent to $\eta \rightarrow 0$ and $\lambda \rightarrow 0$ simultaneously. We then have (see (1)) $|\nabla \cdot \mathbf{Q}|^2 = \left(\frac{dQ_{13}}{dz}\right)^2 + \left(\frac{dQ_{23}}{dz}\right)^2 + \left(\frac{dQ_{33}}{dz}\right)^2 = 0$; recall that the matrix components are labelled by $\mathbf{Q} = (Q_{ij})$ with $i, j = 1, 2, 3$ and hence, minimizers are splay-free with

$$Q'_{13} = Q'_{23} = Q'_{33} = 0, \quad (5)$$

almost everywhere. Assuming a differentiable solution matching the boundary conditions, this implies that $Q_{13} = Q_{23} = 0$ and $Q_{33} = -s_+/3 < 0$, implying that the nematic director is always in the xy -plane. The corresponding leading order energy is

$$F(\mathbf{Q}) = F(\mathbf{q}) = \int_0^1 \left\{ \frac{\eta}{2} |\nabla \mathbf{q}|^2 + 2\sigma \eta (\mathbf{q} \cdot \nabla \times \mathbf{q}) + \frac{\lambda}{C} \tilde{f}_b(s_+, |\mathbf{q}|^2) + C_0(s_+, \eta, \sigma) \right\} dz, \quad (6)$$

where $\mathbf{q} = \left(\frac{Q_{11} - Q_{22}}{2}, Q_{12}\right)$ and C_0 is a function depending on s_+ , η , and σ i.e. there are only two degrees of freedom in the $K_0 \rightarrow \infty$ limit. This limiting model bears considerable similarity to a one-dimensional model studied by Golovaty et al. [29].

Next, we assume that a set of helical states are simultaneously stable, for example \mathbf{Q}_ω , $\omega \in \{n-1, n, n+1\}$. We are interested in pathways between such states, as a minimal model for structural transitions in cholesterics. There is a qualitative difference between an $n-1 \rightarrow n$ transition and $n-1 \rightarrow n+1$. In the first case, the layer number changes by an odd amount, so the transition path must contain a defect because of the conflicting boundary conditions for $\omega = n-1$ and $\omega = n$. In the second case, there is no such constraint and we may expect a defect-free pathway between \mathbf{Q}_{n-1} and \mathbf{Q}_{n+1} .

To compute these pathways, we find minimizing and non-minimizing critical points of the energy, solutions of the Euler-Lagrange equations for (1). The Morse index of a LdG critical point is the number of negative eigenvalues of the corresponding Hessian of the free energy at a critical point [30]. Minimizers (local and global) have index-0, index- k saddle points are unstable in k distinguished eigendirections. Index-1 saddle points are labelled as transition states for switching processes [31]. We use the high-index optimization-based shrinking dimer (HiOSD) method [32] and upward/downward search algorithms [33], to compute sample solution landscapes for this model system, for different values of (η, λ) . We use the Simultaneous Rayleigh-quotient iterative minimization method to calculate the smallest eigenvalues of the Hessian [33] (see SI for more details).

We fix $\sigma = 2\pi$ in the following. We focus on (transition) pathways between \mathbf{Q}_1 (*One*, π twisting) and \mathbf{Q}_3 (*Three*, 3π twisting), which have different chiral invariants, so any pathway must proceed via either untwisting or defects. The *One* and *Three*-helical states have the same energy for any λ , η , and K_0 , and they are stable for η small. For large λ , the uniaxial states \mathbf{Q}_1 , \mathbf{Q}_2 and \mathbf{Q}_3 are energetically preferred. When η is large, the biaxial helix (4) is the limiting minimizer. This raises the following question - are there competing uniaxial and biaxial critical points, with comparable free energies, for finite λ and η and if so, does this facilitate experimental observation of biaxiality? To partially answer this question, we construct an initial condition with 2π twisting in the xy -plane, but with two discontinuous points of the nematic director (see SI). Using Newton's method and this initial condition, we can obtain a splay-free solution labelled as the *Biaxial* solution, for various λ and η . This *Biaxial* solution is not the biaxial helix in (4). The *Biaxial* solution has two biaxial tori around the discontinuous points, and each biaxial torus contains two points of maximal biaxiality (where one eigenvalue of the LdG \mathbf{Q} -tensor vanishes) and a point of uniaxiality at the center. The biaxial torus is a universal defect structure arising from topological constraints [34], and can be understood in terms of eigenvalue exchange. The \mathbf{Q} -tensor can be written as: $\mathbf{Q} = \lambda_1(z)\mathbf{n} \otimes \mathbf{n} + \lambda_2(z)\mathbf{m} \otimes \mathbf{m} - (\lambda_1(z) + \lambda_2(z))\mathbf{z} \otimes \mathbf{z}$, for two mutually orthogonal eigenvectors \mathbf{n} and \mathbf{m} . Informally speaking, the \mathbf{Q} -tensor transitions from $\mathbf{Q}_l = s_+(\mathbf{n} \otimes \mathbf{n} - \frac{I}{3})$ to $\mathbf{Q}_r = s_+(\mathbf{m} \otimes \mathbf{m} - \frac{I}{3})$ keeping the eigenvectors fixed in space, and $\lambda_1 + \lambda_2$ almost fixed (a non-zero constant). One can check that this means that λ_1 and λ_2 must vanish at two separate points inside the biaxial torus, and hence the two points of maximal biaxiality. The constraint of $\lambda_1(l) - \lambda_2(l) > 0$ and $\lambda_1(r) - \lambda_2(r) < 0$, necessarily enforces an almost uniaxial point inside the biaxial torus. For sufficiently small K_0 (when splay is not heavily penalised), the *Biaxial* solution is an unstable saddle point (index > 1), and the Morse index of the *Biaxial* state increases as λ increases.

With the *Biaxial* state as the parent state (state with highest index), we compute the solution landscape for $\lambda = 1$ (corresponding to a relatively small cell of a few hundred nanometers height), and $\eta = 4.5$, shown in Fig. 1. We classify the critical points broadly either as uniaxial and biaxial, and with and without splay (non-zero and zero Q_{13} respectively). We label the critical points as follows: 'B' indicates the presence of biaxial tori, 'Z' indicates that $q_3 \equiv Q_{13}$ is non-zero, and the number at the end is the amount of rotation in the xy -plane, in units of π radians. With $\lambda = 1$, $\eta = 4.5$, the *Biaxial(B2)* state is index-4. The *B2*, state with two biaxial tori, has unstable directions that tune the twisting periods and connect with both the stable *One* and *Three* states. Following the unstable eigendirections, the *Biaxial* state connects with three index-2 critical points, *B1.5*, *B2.5*, and *BBZ2*. *B1.5* and *B2.5* have only one biaxial torus, with $3\pi/2$ and $5\pi/2$ twisting respectively. The saddle

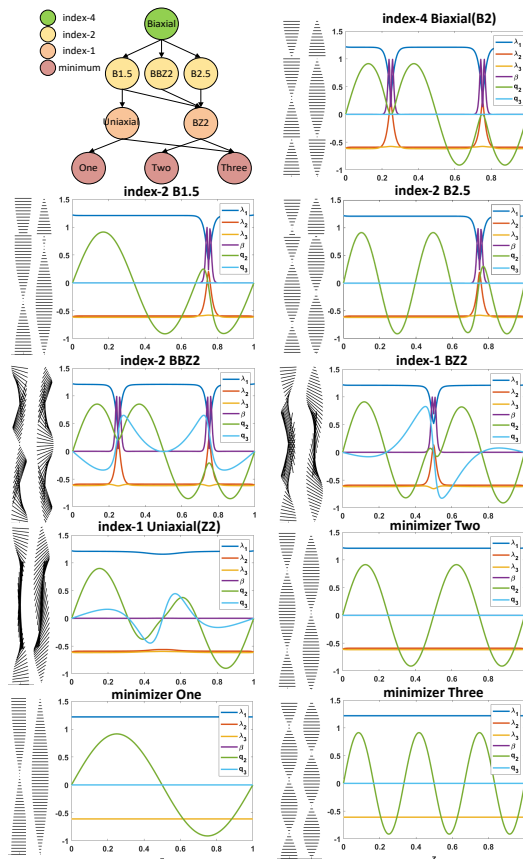


FIG. 1: The solution landscape with $\lambda = 1$, $\eta = 4.5$, $\sigma = 2\pi$. We use $A = -B^2/3C$, $B = 0.64 \times 10^4 N/m^2$ and $C = 0.35 \times 10^4 N/m^2$. We plot the eigenvector corresponding to the largest eigenvalue of the \mathbf{Q} -solution, the three eigenvalues $\lambda_1 \geq \lambda_2 \geq \lambda_3$, the biaxiality measure $\beta = 1 - 6 \frac{(\text{tr} \mathbf{Q}^3)^2}{|\mathbf{Q}|_0^3}$, $q_2 \equiv Q_{12}$ and the splay measure, q_3 , on the right. The *One*, *Two* and *Three*-helical uniaxial solutions are stable for these parameters.

points, *B1.5* and *B2.5*, connecting the helical states *One* and *Two*, and *Two* and *Three* respectively, must contain biaxial tori (defects). *BBZ2* has a more complex profile with two biaxial tori, 2π twisting, and splay pattern. Finally, we also find the defect-free index-1 *Uniaxial(ZZ)* state, which is the transition state between the stable *One* and *Three* states. *BZ2* is the transition state between the stable *Two* and *Three* helical states, we could not find a transition state between the *One* and *Two*-helical states.

We find, therefore, two competing qualitatively distinct pathways between the stable uniaxial *One* and *Three*-helical states. According to Figure 1, there is an uniaxial pathway via the index-1 *Uniaxial* state, and the biaxial pathway via the index-4 *Biaxial* state. Contact topology results [8, 10, 21] imply that the uniaxial pathway must untwist (i.e. have $\mathbf{n} \cdot \nabla \times \mathbf{n} = 0$ at some point, the center of the cell in the case of *Uniaxial(ZZ)*), this untwisting is mediated by splay. On the other hand, the biaxial state, *B2*, is splay-free and indeed the entire

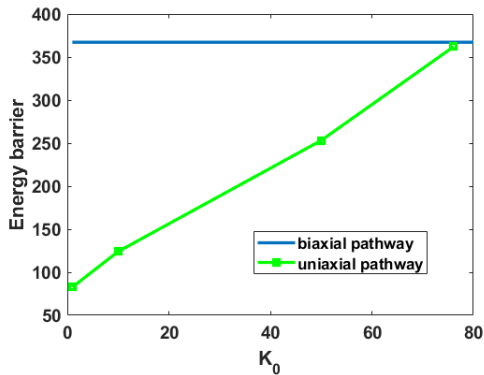


FIG. 2: The energy barriers for the uniaxial and biaxial pathways vs K_0 , with re-scaled energy $K_0 F$, F in (1).

pathway in this case can be chosen in the class of splay-free configurations (6). The system can choose between splay or biaxiality along the pathway (note that the BZ critical points contain both splay *and* biaxiality), and the selection of the pathway depends on the elastic constants. In the $K_0 \rightarrow \infty$ limit, (1), the splay-free states: *Biaxial(B2)*, *B1.5*, *B2.5*, uniaxial *One*, *Two*, and *Three* states, survive as critical points of the free energy. In particular, the *Biaxial* state is always a critical point of (1) for all K_0 , and the index of *Biaxial* state decreases from 4, to 3, to 2, to 0, as K_0 increases from 1 to ∞ . The *Uniaxial(Z2)*, *BZ2*, and *BBZ2*, have splay patterns i.e., they become energetically expensive and their Morse index increases with K_0 . The biaxial torus is a recurring structural motif and we observe that the index of the biaxial critical points is twice the number of biaxial tori in the splay-free case, and equal to the number of biaxial tori with splay in Figure 1. In general, the relationship between the number of biaxial tori (defects), splay and the index depends on λ and η . The energy barrier of the pathway is the energy difference between either the *Uniaxial(Z2)* or *Biaxial(B2)* critical point, and the stable *One* (or *Three*) states. Hence as K_0 increases, the energy barrier of the biaxial pathway does not change (since the energy of the *Biaxial* critical point is independent of K_0), but the energy barrier of the uniaxial transition pathway increases, see Figure 2. The *Uniaxial* critical point ceases to exist for $K_0 > 76.1$. For $K_0 < 76.1$, the energy barrier for the uniaxial pathway is always lower than that of the biaxial pathway, but the barriers become comparable at $K_0 = 76.1$. Hence, in this specific case of $\lambda = 1$ and $\eta = 4.5$, the uniaxial pathway cannot be observed for large K_0 , and equally importantly, the uniaxial and biaxial transition pathways have comparable energy barriers for sufficiently large K_0 . Hence, there is no obvious reason for the system to always choose the uniaxial pathway, and we conjecture that the *Biaxial(B2)* critical point may be experimentally observable in these regimes of finite λ, η and sufficiently large K_0 .

What are the implications for experiments? During

coarsening or other dynamic processes (for example, the Helfrich-Huraulty instability [35]) cholesterics will typically undergo morphological changes whereby ‘layer numbers’ are observed to change in a discrete fashion. Our work suggests that a cholesteric system can choose to mediate such a transition by either untwisting via splay, or through biaxiality (defects). Experimentally verifiable optical signatures for these states as well as their pathways, computed using the Jones Matrix formalism, are shown in the SI.

Our findings illustrate that biaxiality may become experimentally observable for these toy systems, with large η and large K_0 , either as equilibria or in (transition) pathways between distinct equilibria. Further, we conjecture that we can construct hierarchies of LdG critical points from building points e.g. the biaxial torus, and the natural periodicity of cholesteric systems implies that such repeating structures could be stable in certain settings. We expect the landscape to be increasingly complex with increasing λ , and conflicting boundary conditions, and in fact, cholesteric states with defects (biaxial tori) are expected to be energy minimizing for certain model problems [34]. In higher dimensions cholesterics typically exhibit great complexity, with tremendous scope for transition pathways and switchable devices and our major challenge is to discover universal principles for solution landscapes of confined soft matter systems, dictated by the order parameter and the free energy.

Acknowledgements: AM, JD and YH gratefully acknowledge support from a Heilbronn Small Grant that facilitated this collaboration. AM is also supported by the University of Strathclyde New Professors Fund, a Leverhulme International Academic Fellowship, an OCIAM Visiting Fellowship at the University of Oxford and a Daiwa Foundation Small Grant. JD acknowledges support from the University of Strathclyde and the DST-UKIERI. YH is supported by a Royal Society Newton International Fellowship. TM and BMGDC acknowledge funding from EPSRC with grant code EP/L016648/1.

I. SUPPLEMENTARY INFORMATION

A. Computational Methods

We construct the initial condition of *Biaxial(B2)* as follows

$$\begin{aligned} \mathbf{Q}(z) &= s_+ \left(\mathbf{n} \otimes \mathbf{n} - \frac{1}{3} \mathbf{I} \right) \\ &= \begin{cases} \mathbf{Q}_2(z), & z \in (0, 0.25) \cup (0.75, 1) \\ S\mathbf{Q}_2(z)S^T, & z \in (0.25, 0.75), \end{cases} \end{aligned}$$

where S is the rotation matrix which rotates the state on $z \in (0.25, 0.75)$ by 90 degree in the xy -plane. The initial condition has 2π twisting, but with two discontinuous points of the nematic director \mathbf{n} , at $z = 0.25$ and 0.75 , and the director flips by 90 degrees at these points.

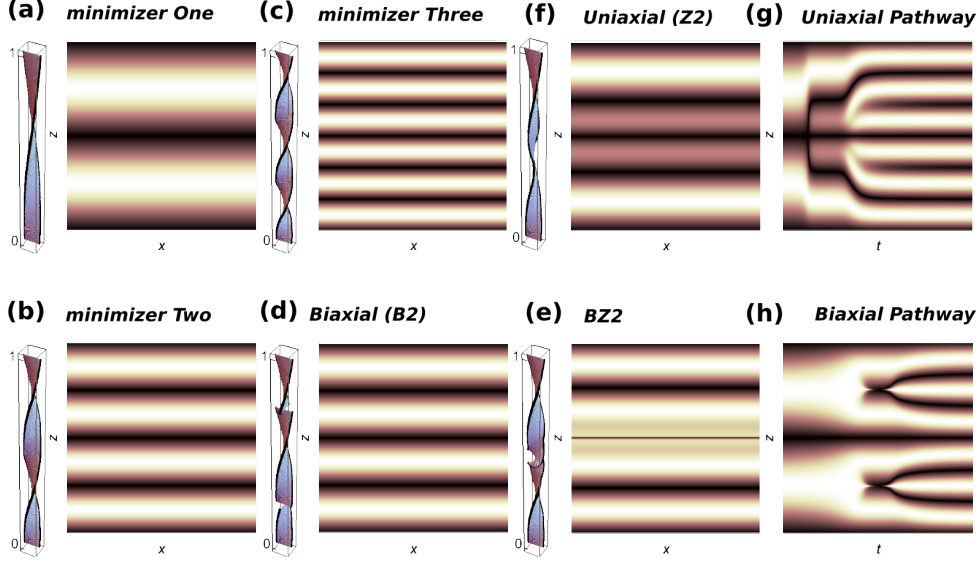


FIG. 3: Optical signatures for a set of metastable states (a), (b), (c); and transition states (f), (d), (e). (g) (h) show space-time optical signatures for the uniaxial and biaxial pathways.

The high-index optimization-based shrinking dimer (HiOSD) method [32] is a local-search algorithm for the computation of saddle point of arbitrary indices, which can be viewed as a generalization of the optimization-based shrinking dimer method for searching index-1 saddle points [36]. It is an efficient tool for constructing the solution landscape searching from high- or low-index saddle points and revealing the connectivity of saddle points and minimizers.

For a non-degenerate index- k saddle point $\hat{\mathbf{Q}}$, the Hessian $\mathbb{H}(\mathbf{Q}) = \nabla^2 F(\mathbf{Q})$ at $\hat{\mathbf{Q}}$ has exactly k negative eigenvalues $\hat{\lambda}_1 \leq \dots \leq \hat{\lambda}_k$ with corresponding unit eigenvectors $\hat{\mathbf{v}}_1, \dots, \hat{\mathbf{v}}_k$ satisfying $\langle \hat{\mathbf{v}}_j, \hat{\mathbf{v}}_i \rangle = \delta_{ij}$, $1 \leq i, j \leq k$. Define a k -dimensional subspace $\hat{\mathcal{V}} = \text{span}\{\hat{\mathbf{v}}_1, \dots, \hat{\mathbf{v}}_k\}$, then $\hat{\mathbf{Q}}$ is a local maximum on a k -dimensional linear manifold $\hat{\mathbf{Q}} + \hat{\mathcal{V}}$ and a local minimum on $\hat{\mathbf{Q}} + \hat{\mathcal{V}}^\perp$, where $\hat{\mathcal{V}}^\perp$ is the orthogonal complement space of $\hat{\mathcal{V}}$.

The k -dimensional subspace $\hat{\mathcal{V}}$ is constructed by solving the following constrained optimization problem using gradient flow,

$$\min_{\mathbf{v}_i \in \mathbb{R}^n} \langle \mathbb{H}(\mathbf{Q})\mathbf{v}_i, \mathbf{v}_i \rangle, \quad \text{s.t.} \quad \langle \mathbf{v}_j, \mathbf{v}_i \rangle = \delta_{ij}, \quad j = 1, 2, \dots, i. \quad (7)$$

The k -index $\hat{\mathbf{Q}}$ can be achieved by a minimax optimization problem

$$\min_{\mathbf{Q}_{\hat{\mathcal{V}}^\perp} \in \hat{\mathcal{V}}^\perp} \max_{\mathbf{Q}_{\hat{\mathcal{V}}} \in \hat{\mathcal{V}}} F(\mathbf{Q}_{\hat{\mathcal{V}}^\perp} + \mathbf{Q}_{\hat{\mathcal{V}}}), \quad (8)$$

where $\mathbf{Q}_{\hat{\mathcal{V}}} = \mathcal{P}_{\hat{\mathcal{V}}}\mathbf{Q}$ is the orthogonal projection of \mathbf{Q} on $\hat{\mathcal{V}}$, and $\mathbf{Q}_{\hat{\mathcal{V}}^\perp} = \mathbf{Q} - \mathcal{P}_{\hat{\mathcal{V}}}\mathbf{Q}$.

Thus with the simultaneous Rayleigh-quotient iterative minimization method, a dynamical system of the

HiOSD is developed for finding an index- k saddle point,

$$\begin{cases} \beta^{-1} \dot{\mathbf{Q}} = - \left(\mathbf{I} - 2 \sum_{j=1}^k \mathbf{v}_j \mathbf{v}_j^\top \right) \nabla F(\mathbf{Q}), \\ \gamma^{-1} \dot{\mathbf{v}}_i = - \left(\mathbf{I} - \mathbf{v}_i \mathbf{v}_i^\top - 2 \sum_{j=1}^{i-1} \mathbf{v}_j \mathbf{v}_j^\top \right) \mathbb{H}(\mathbf{Q})\mathbf{v}_i, \quad i = 1, \dots, k, \end{cases} \quad (9)$$

where the state variable \mathbf{Q} and k direction variables \mathbf{v}_i are coupled, \mathbf{I} is the identity operator and $\beta, \gamma > 0$ are relaxation parameters.

B. Optical Modelling

In order to predict the optical motifs, we use the Jones Matrix formalism; which considers the theoretical optical transmission of a plane wave of normal incidence through a twisted nematic material. The incident wave is modelled as propagating in the \mathbf{e}_y direction. The cholesteric is considered as a collection of nodes with a specific magnitude of birefringence depending on the local orientation of the director field with respect to the incident wave. Using the 2×2 Jones Matrix formalism, we calculate the output of the field, E^o as

$$\begin{pmatrix} E_x^o \\ E_z^o \end{pmatrix} = \begin{pmatrix} 0 & 0 \\ 0 & 1 \end{pmatrix} \mathbf{J} \begin{pmatrix} 1 & 0 \\ 0 & 0 \end{pmatrix} \begin{pmatrix} E_x^i \\ E_z^i \end{pmatrix} \quad (10)$$

where E^i is the magnitude of the incident wave in the specified directions and \mathbf{J} is the Jones matrix as given by

$$\mathbf{J} = \begin{pmatrix} \cos^2(\gamma)e^{i\phi_e} + \sin^2(\gamma)e^{i\phi_0} & \cos(\gamma)\sin(\gamma)(e^{i\phi_e} - e^{i\phi_0}) \\ \cos(\gamma)\sin(\gamma)(e^{i\phi_e} - e^{i\phi_0}) & \sin^2(\gamma)e^{i\phi_e} + \cos^2(\gamma)e^{i\phi_0} \end{pmatrix}. \quad (11)$$

The wavelength of the incident beam, λ , is considered to be $\lambda = 450\text{nm}$, γ represents the azimuthal angle between the extraordinary axis and the alignment of the director at the walls, (\mathbf{e}_x), and ϕ_0 and ϕ_e are the ordinary and extraordinary phase shifts, respectively, induced by the nematic where

$$\phi_0 = \frac{2\pi}{\lambda} n_0 \quad (12)$$

$$\phi_e = \frac{2\pi}{\lambda} n_e(\beta). \quad (13)$$

In this case we consider $n_0 = 1.52$ being the ordinary refractive index of the cholesteric and $n_e(\beta)$ being the local extraordinary index determined by

$$n_e^2(\beta) = \frac{n_0 n_e}{\sqrt{n_0^2 \sin^2(\beta) + n_e^2 \cos^2(\beta)}} \quad (14)$$

which is dependent upon the extraordinary refractive index of the material; in this case $n_e = 1.90$; and β being the angle between the incident wave (\mathbf{e}_y direction) and the local director.

In experiments, these transmission profiles are studied via optical microscopy [37]. The numerically computed transmission profiles for the uniaxial critical points, with splay, are distinguished via distinct motifs with broadly distributed peaks that are fractured by localised ‘dark’ regions. We note that the optical signature of the index-4 *Biaxial* state (*B2*) is indistinct from the optical signature of the doubly twisted metastable state (Minimizer Two), possibly because the Jones matrix is inherently uniaxial and cannot capture biaxiality.

-
- [1] Uroš Tkalec, Miha Ravnik, Simon Čopar, Slobodan Žumer, and Igor Mušević. Reconfigurable knots and links in chiral nematic colloids. *Science*, 333(6038):62–65, 2011.
- [2] Jung-Shen B Tai and Ivan I Smalyukh. Three-dimensional crystals of adaptive knots. *Science*, 365(6460):1449–1453, 2019.
- [3] Thomas Machon and Gareth P Alexander. Knotted defects in nematic liquid crystals. *Phys. Rev. Lett.*, 113(2):027801, 2014.
- [4] Thomas Machon and Gareth P Alexander. Knots and nonorientable surfaces in chiral nematics. *Proc. Natl. Acad. Sci. USA*, 110(35):14174–14179, 2013.
- [5] Ivan I Smalyukh, Yves Lansac, Noel A Clark, and Rahul P Trivedi. Three-dimensional structure and multistable optical switching of triple-twisted particle-like excitations in anisotropic fluids. *Nat. Mater.*, 9(2):139–145, 2010.
- [6] Bryan Gin-ge Chen, Paul J Ackerman, Gareth P Alexander, Randall D Kamien, and Ivan I Smalyukh. Generating the hopf fibration experimentally in nematic liquid crystals. *Phys. Rev. Lett.*, 110(23):237801, 2013.
- [7] Paul J Ackerman and Ivan I Smalyukh. Diversity of knot solitons in liquid crystals manifested by linking of preimages in torons and hopfions. *Phys. Rev. X*, 7(1):011006, 2017.
- [8] Jonghee Eun, Joseph Pollard, Sung-Jo Kim, Thomas Machon, and Joonwoo Jeong. Layering transitions and metastable structures of cholesteric liquid crystals in cylindrical confinement. *Proc. Natl. Acad. Sci. USA*, 118(33), 2021.
- [9] Gregor Posnjak, Simon Čopar, and Igor Mušević. Hidden topological constellations and polyvalent charges in chiral nematic droplets. *Nat. Commun.*, 8(1):1–9, 2017.
- [10] Joseph Pollard, Gregor Posnjak, Simon Čopar, Igor Mušević, and Gareth P Alexander. Point defects, topological chirality, and singularity theory in cholesteric liquid-crystal droplets. *Phys. Rev. X*, 9(2):021004, 2019.
- [11] Alexandre Darmon, Michael Benzaquen, Simon Čopar, Olivier Dauchot, and Teresa Lopez-Leon. Topological defects in cholesteric liquid crystal shells. *Soft Matter*, 12(46):9280–9288, 2016.
- [12] Yves Bouligand and Françoise Livolant. The organization of cholesteric spherulites. *J. Phys. (Paris)*, 45(12):1899–1923, 1984.
- [13] Alexandre Darmon, Michael Benzaquen, David Seč, Simon Čopar, Olivier Dauchot, and Teresa Lopez-Leon. Waltzing route toward double-helix formation in cholesteric shells. *Proc. Natl. Acad. Sci. USA*, 113(34):9469–9474, 2016.
- [14] Lisa Tran, Maxim O Lavrentovich, Guillaume Durey, Alexandre Darmon, Martin F Haase, Ningwei Li, Daeyeon Lee, Kathleen J Stebe, Randall D Kamien, and Teresa Lopez-Leon. Change in stripes for cholesteric shells via anchoring in moderation. *Phys. Rev. X*, 7(4):041029, 2017.
- [15] Jun-ichi Fukuda and Slobodan Žumer. Quasi-two-dimensional skyrmion lattices in a chiral nematic liquid crystal. *Nat. Commun.*, 2(1):1–5, 2011.
- [16] EC Gartland, H Huang, OD Lavrentovich, P Palffy-Muhoray, II Smalyukh, T Kosa, and B Taheri. Electric-field induced transitions in a cholesteric liquid-crystal film with negative dielectric anisotropy. *J. Comput. Theor. Nanosci.*, 7(4):709–725, 2010.
- [17] Yucen Han, Jianyuan Yin, Pingwen Zhang, Apala Majumdar, and Lei Zhang. Solution landscape of a reduced landau–de gennes model on a hexagon. *Nonlinearity*, 34(4):2048, 2021.
- [18] N David Mermin. The topological theory of defects in ordered media. *Rev. Mod. Phys.*, 51(3):591, 1979.
- [19] Gareth P Alexander, Bryan Gin-ge Chen, Elisabetta A Matsumoto, and Randall D Kamien. Colloquium: Disclination loops, point defects, and all that in nematic liquid crystals. *Rev. Mod. Phys.*, 84(2):497, 2012.
- [20] Valentin Poenaru and Gérard Toulouse. The crossing of defects in ordered media and the topology of 3-manifolds. *J. Phys. (Paris)*, 38(8):887–895, 1977.
- [21] Thomas Machon. Contact topology and the structure and dynamics of cholesterics. *New. J. Phys.*, 19(11):113030, 2017.
- [22] Hansjörg Geiges. *An introduction to contact topology*, volume 109. Cambridge University Press, 2008.
- [23] Yichen Hu and Thomas Machon. Stability of highly-twisted skyrmions from contact topology.

- arXiv:2102.13126*, 2021.
- [24] P. G. de Gennes. *The Physics of Liquid Crystals*. Oxford University Press, Oxford, 1974.
- [25] Junichi Fukuda and S Žumer. Cholesteric blue phases: effect of strong confinement. *Liq. Cryst.*, 37(6-7):875–882, 2010.
- [26] A. Majumdar. Equilibrium order parameters of nematic liquid crystals in the Landau–de Gennes theory. *Euro. J. Appl. Math.*, 21:181–203, 2010.
- [27] David C Wright and N David Mermin. Crystalline liquids: the blue phases. *Rev. Mod. Phys.*, 61(2):385, 1989.
- [28] Apala Majumdar and Arghir Zarnescu. Landau–de gennes theory of nematic liquid crystals: the oseen–frank limit and beyond. *Arch. Ration. Mech. Anal.*, 196(1):227–280, 2010.
- [29] Dmitry Golovaty, Michael Novack, and Peter Sternberg. A one-dimensional variational problem for cholesteric liquid crystals with disparate elastic constants. *J. Differ. Equ.*, 286:785–820, 2021.
- [30] J Milnor. *Morse Theory*. Princeton University Press, Princeton, NJ, 1963.
- [31] Halim Kusumaatmaja and Apala Majumdar. Free energy pathways of a multistable liquid crystal device. *Soft Matter*, 11(24):4809–4817, 2015.
- [32] JY Yin, L Zhang, and PW Zhang. High-index optimization-based shrinking dimer method for finding high-index saddle points. *SIAM J. Sci. Comput.*, 41(6):A3576–A3595, 2019.
- [33] JY Yin, YW Wang, JZY Chen, PW Zhang, and L Zhang. Construction of a pathway map on a complicated energy landscape. *Phys. Rev. Lett.*, 124:090601, 3 2020.
- [34] Duvan Henao, Apala Majumdar, and Adriano Pisante. Uniaxial versus biaxial character of nematic equilibria in three dimensions. *Calc. Var. Partial Differ. Equ.*, 56(2):55, 2017.
- [35] Christophe Blanc, Guillaume Durey, Randall D Kamien, Teresa Lopez-Leon, Maxim O Lavrentovich, and Lisa Tran. Helfrich-hurault elastic instabilities driven by geometrical frustration. *arXiv:2109.14668*, 2021.
- [36] Lei Zhang, Qiang Du, and Zhenzhen Zheng. Optimization-based shrinking dimer method for finding transition states. *SIAM J. Sci. Comput.*, 38(1):A528–A544, 2016.
- [37] Paul S Drzaic. *Liquid Crystal Dispersions*. World Scientific, 1995.